Supplementary Information

Topological Defects in Liquid Crystals as Templates for Molecular Self-Assembly

Xiaoguang Wang[1], Daniel S. Miller[1], Emre Bukusoglu[1], Juan J. de Pablo[2], and Nicholas L. Abbott[1*]

1. Department of Chemical and Biological Engineering, University of Wisconsin-Madison, Madison, WI 53706-1691 USA.
2. Institute for Molecular Engineering, University of Chicago, Chicago, Illinois 60637 USA.

[*]To whom correspondence may be addressed. E-mail: abbott@engr.wisc.edu.

Table of Contents:

Methods

Exposure times used in fluorescence microscopy.

Table S1. Exposure times used to collect images shown in Fig. 2, Fig. S4 and S5:

Amphiphile	Exposure time (s)	
	λ^{em}: 510-562 nm	λ^{em}: 606-684 nm
BODIPY	0.003	0.2
BODIPY-C5	0.003	0.1
BODIPY-C12	0.005	0.12
BODIPY-C16	0.01	0.15
BODIPY-DHPE	0.3 (0.19-1.9 μM) 0.1 (3-9.6 μM)	1 (0.19-1.9 μM) 0.3 (3-9.6 μM)

Table S2. Exposure times used to collect data in Fig. 3:

BODIPY-fatty acids Concentration (μM)	Exposure time (s)
	λ^{em}: 606-684 nm
19-57	0.1
95	0.05
140-190	0.04
285-950	0.025

Table S3. Exposure times used to collect data in Fig. S3:

BODIPY Concentration (μM)	Exposure time (s)	
	λ^{em}: 510-562 nm	λ^{em}: 606-684 nm
9.5	0.003	0.2
190	0.002	0.1
380-570	0.0005	0.05
760-950	0.0003	0.03

Results

Absorption and emission properties of BODIPY-amphiphiles. To facilitate the interpretation of fluorescence micrographs of the BODIPY-amphiphiles presented in the main text, we characterized the absorption and emission spectra of BODIPY-amphiphiles. As stated above and in the main text, we used two different filter sets on our fluorescence microscope to characterize the state of assembly of the BODIPY-labeled amphiphiles. Filter set 1 was comprised of an excitation filter that transmitted light with wavelengths between 457 nm and 502 nm (λ^{ex}: 457-502 nm) and an emission filter that transmitted light with wavelengths of 510 nm to 562 nm (λ^{em}: 510-562 nm). Filter set 2 used excitation and emission filters that transmitted light with wavelengths of 533 nm to 584 nm (λ^{ex}: 533-584 nm) and 606 nm to 684 nm (λ^{em}: 606-684 nm), respectively. Below, we describe how the state of assembly of the BODIPY-labeled amphiphiles influences the fluorescence intensity that is quantified using each filter set.

We characterized the absorption and emission properties of the BODIPY-amphiphiles in three different solvent systems, namely water, ethanol and isotropic 5CB. These solvents were selected because they generated different states of association of the BODIPY-amphiphiles, and thus they allowed us to understand changes in optical properties of the compounds that accompany changes in the state of assembly. Fig. S2a (black line) shows the absorption spectra of BODIPY-C5 in ethanol. The singly dispersed state of the amphiphile is characterized by the absorption maximum at 500 nm [1]. We also observed BODIPY-C5 to assume a singly dispersed state in water and isotropic 5CB. The latter is evidenced by the absorption maximum at 512 nm (i.e., red-shifted relative to water and ethanol) in Fig. S2d. The effects of self-association on the absorption spectra of the BODIPY-amphiphiles are illustrated in Fig. S2a, showing BODIPY-C12 in water (red line) and BODIPY-DHPE in water (blue line). Additional measurements of absorption spectra (not shown) also revealed that at a concentration of 3.8 μM, no BODIPY amphiphiles self-associated in either ethanol or isotropic 5CB, but that BODIPY-C16 self-associated in water. Below we discuss the fluorescence signal generated by the singly-dispersed (so-called monomeric signal) and assembled states (so-called dimeric signal) of the BODIPY amphiphiles when using λ^{em} 510-562 nm and 606-684 nm in the microscope. The discussion below pertains to solutions that contained the same concentration of BODIPY amphiphiles (3.8 μM).

Fig. S2b and e address the fluorescent signal generated when using λ^{em}: 510-562 nm. Specifically, Fig. S2b and e show the emission spectra from the BODIPY-amphiphiles when excited with light with wavelengths of 464-494 nm (similar to excitation filter with λ^{ex} 457-502 nm). Also indicated in Fig. S2b and e is the range of wavelengths that correspond to the emission filter of λ^{em} 510-562 nm. Inspection of these two figures reveals that the singly dispersed BODIPY-amphiphiles give rise to a substantial intensity of emitted light that passes through the emission filter of λ^{em}: 510-562 nm, but that the assembled states of the BODIPY-amphiphiles give rise to only very weak emission with λ^{em}: 510-562 nm. Here we note, however, that the emission spectrum of BODIPY-DHPE assemblies shows a stronger peak in the range of the emission filter λ^{em} 510-562 nm (Fig. S2b) as compared to the BODIPY-fatty acid assemblies. This result indicates that BODIPY-DHPE should generate a substantial intensity of emitted light that passes through filters at λ^{em} 510-562 nm and 606-684 nm. We also note here that at the same concentration, the intensity of fluorescence of BODIPY-fatty acids was approximate 10 times that of BODIPY-DHPE (Fig. S2b, c, e and f).

Fig. S2c and f address the fluorescent signal generated when using λ^{em}: 606-684 nm. Specifically, Fig. S2c and f show the emission from the BODIPY-labeled amphiphiles when excited with light with wavelengths of 544-574 nm (similar to excitation filter with λ^{ex} 533-584 nm). Inspection of Fig. S2c and f reveal that both singly dispersed and assembled states of the BODIPY-labeled amphiphiles give rise to an intensity of fluorescence with wavelengths that coincide with the emission filter of λ^{em} 606-684 nm (indicated in the figures). It is also evident, however, that the intensity of fluorescence is greater for the assembled states of the BODIPY-labeled amphiphiles than their singly dispersed state.

In summary, the results above indicate that the fluorescence signal from λ^{em} 510-562 nm will be generated largely from singly dispersed BODIPY molecules whereas λ^{em} 606-684 nm will contain contributions from both singly dispersed and assembled states of the amphiphiles but with a dominant contribution coming from assembled states. We note here that the monomeric emission spectrum overlaps with the adsorption spectrum of assemblies of BODIPY amphiphiles (see Fig. S2), which might complicate our quantification. Next, we calculate the absorption of light by BODIPY assemblies in LC defects. The Beer Lambert law can be written as[2]:

$$ebC = \log(I_0/I) \quad \text{(S1)}$$

in which e is the molar absorptivity, b is the path length, C is the concentration of the compound in the solution, and I_0 and I are the intensities of incident beam and transmitted beam, respectively. From Fig. S2a (using λ = 525 nm, which corresponds to the maximum in the monomer emission, see Fig. S2b), e is estimated to be 2.1×10^5 L/(mol m) (c is 3.8 μM, b is ~ 5 mm, and $\log(I_0/I)$ is ~ 0.04).

The concentration of BODIPY amphiphiles in assemblies within the LC defects ($C_{amphiphile\text{-}in\text{-}defect}$) is estimated to be 1.6 M, which is equivalent to the concentration of pure amphiphiles (assuming the molecular volume per amphiphile to be ~ 1 nm^3). With the values of e and $C_{amphiphile\text{-}in\text{-}defect}$ (see above), we calculate the transmittance of an incident beam through a 10 nm-thick assembly using equation (S2) to be I/I_0 ~ 99.2%. Thus, we conclude that light emitted by the monomer is absorbed negligibly by BODIPY amphiphiles in assemblies in the system.

Proportionality of fluorescence intensity to exposure time and concentration of fluorophore. In Fig. S3, using BODIPY, we confirmed that the rescaled fluorescence intensity was linearly proportional to both exposure time and concentration of fluorophore for the range of exposure times and concentrations used in the present study (10-950 μM).

State of BODIPY in LCs. The rescaled fluorescence intensities of BODIPY in the bulk LC and defects are shown in Fig. S3. When using either λ^{em}: 510-562 nm or λ^{em}: 606-684, no measurable difference between the fluorescence intensity of the defect and the bulk of the nematic phase was detected over a wide concentration range (10-950 μM). In addition, the fluorescence intensities measured using both filter sets in the bulk LC phase increased linearly with the concentration of BODIPY. This behavior is consistent with the presence of singly dispersed BODIPY molecules in both the bulk of the nematic phase and the defects. Overall, this result indicates that BODIPY distributed uniformly between the bulk of the LC and defects.

State of BODIPY-DHPE in LCs. In this section, we characterized the behavior of the double-tailed amphiphile BODIPY-DHPE (see Fig. 1c in the main text for molecular structure). Similar to the BODIPY-fatty acids (Fig. 2h in the main text), we observed BODIPY-DHPE to exhibit a

CAC of 1.5 μM within the -1/2 line defects of the nematic LC (Fig. S5 and Fig. 2i in the main text). In contrast to BODIPY-fatty acids, however, we observed BODIPY-DHPE to also exhibit a CAC in the bulk of the LC. The CAC in the bulk was 5.5 μM, and thus higher than that measured in the environment of the defect. We comment here that above the CAC, a significant difference in the fluorescence intensity was detected for both filter sets. This is because the emission spectrum of BODIPY-DHPE assemblies shows a strong peak in the range of the emission filter λ^{em} 510-562 nm (see Fig. S2e and above for detail discussion). The observation of two CACs for BODIPY-DHPE is thus analogous to that reported previously for the self-assembly of surfactants in the presence of hydrophobically-modified polymers[3-9]. We comment here also that the assemblies of amphiphiles formed in the bulk LC tended to be expelled from the bulk LC (e.g., towards surfaces) over time.

Contribution of "core replacement" energy to ΔG_1^0. In addition to the role of the chain entropy in driving self-assembly (see main text), we also evaluated the role of the defect core energy in driving the self-assembly process. The "core replacement" contribution was estimated to be ~ 10^3 k_BT for transfer of a 10 nm-in-length assembly from the bulk LC to the defect ($\mathcal{E}v_{assembly}$, in which $\mathcal{E}$ is the free energy of "melting" the nematic phase (0.65 kJ/mol[10]) and $v_{assembly}$ is the volume of the assembly (10 nm-in-length and 10 nm-in-diameter)). By assuming the volume of a methylene group in an aliphatic chain to be ~ 26.9 Å^3 [11], we estimate the free energy gain associated with replacement of the defect core to be ~0.04 k_BT/methylene. This calculation leads us to conclude that self-assembly of amphiphiles within LC defects is driven by the free energy gain associated with both amphiphile tail entropy (see main text) and replacement of the mesogens in the cores of LC defects by amphiphilic assemblies.

Contribution of interfacial tension to ΔG_1^0. In addition to evaluating the role of chain entropy and "core replacement", we also considered the role of interfacial tension between the nematic bulk and the isotropic defect core in driving the self-assembly process. The interfacial tension contribution was estimated to be ~ 1 k_BT for transfer of a 10 nm-in-length assembly from the bulk LC to the defect ($\gamma S_{assembly}$, in which γ is the interfacial tension between the nematic and isotropic phase of 5CB (10 μJ/m^2) [12], and $S_{assembly}$ is the surface area of the assembly (10 nm-in-length and 10 nm-in-diameter)), which is three orders of magnitude smaller than the "core

replacement" and chain entropy contribution to the standard free energy (see above and main text). This analysis leads us to conclude that the contribution of the interfacial tension to the standard free energy of transfer can be neglected.

Reversible assembly and disassembly of amphiphilic molecules in LC defects. As shown in Fig. 5a and b in the main text, the "Saturn-ring" defect region exhibits more intense fluorescence signal than the bulk. After the system was heated into the isotropic phase to erase the defects (Fig. 5d and e), homogeneous fluorescence intensity was detected throughout the volume of the system, which indicates that the molecular assemblies disassembled and the amphiphiles dispersed into isotropic bulk LC. This result demonstrates that the defect-directed assembly of amphiphiles is reversible.

Thermodynamic model for molecular self-assembly in LC defects. Our experimental observations suggest that the self-assembly of amphiphiles in defects has many analogies to cooperative self-assembly of amphiphiles with hydrophobically-modified polymers in water. Here we sought to derive a simple thermodynamic model to describe key features of the concentration-dependent monomeric and dimeric signals shown in Figure 4a and b. In Section 1 and 2, we describe a model for formation of free micelles in the absence of hydrophobically-modified polymers according to References 2 and 11. In Section 3 and 4, we present a model for a system containing surfactants and hydrophobically modified polymers, which can form polymer—surfactant complexes in addition to free micelles according to Reference 13 and 14. In Section 5, we adapt these models to describe the self-assembly of amphiphiles in topological defects in LCs.

Section 1. Formation of micelles.

The formation of micelles can be described stepwise as:

$$X_1 + X_1 \overset{k_f}{\leftrightarrow} X_2 \tag{S2}$$

$$X_1 + X_2 \overset{k_f}{\leftrightarrow} X_3 \tag{S3}$$

……

and overall process can be written as:

$$g_f X_1 \overset{k_1}{\leftrightarrow} X_f \tag{S4}$$

where X_1 denotes singly dispersed surfactant, X_f denotes micelles with aggregation number g_f, k_f is the equilibrium constant for each step (which is assumed to be constant), and k_1 is an equilibrium constant for the overall process of formation of micelles.

From equation (S4), we can write:

$$k_1 = \frac{[X_f]}{[X_1]^{g_f}} \tag{S5}$$

where [] denotes the volumetric concentration of each species. The concentration of surfactant molecules in the micellar state $[X_{micelle}]$ can be calculated for g_f>>1 as:

$$[X_{micelle}] = g_f[X_f] = g_f k_1 [X_1]^{g_f} \approx g_f (k_f [X_1])^{g_f} \tag{S6}$$

Thus, the total concentration of all amphiphiles ($[X_{total}]$) can be written as:

$$\begin{aligned} [X_{total}] &= [\text{singly dispersed surfactant}] + [\text{surfactant in micelles}] \\ &= [X_1] + [X_{micelle}] \\ &= [X_1] + g_f (k_f [X_1])^{g_f} \end{aligned} \tag{S7}$$

Section 2. Derivation of ΔG_1^0 for formation of free micelles.

The relationship between standard free energy and equilibrium constant can be written as:

$$k_1 = e^{-\frac{\Delta G^o}{kT}} \tag{S8}$$

or alternatively

$$\Delta G^o = -kTlnk_1 \tag{S9}$$

Substitution of equation (S6) into (S9) leads to:

$$\begin{aligned} \Delta G^o &= -kTln\frac{[X_f]}{[X_1]^{g_f}} \\ &= g_f kTln[X_1] - kTln[X_f] \end{aligned} \tag{S10}$$

By dividing by g_f on both sides, we obtain:

$$\frac{\Delta G^o}{g_f} = kTln[X_1] - \frac{kTln[X_f]}{g_f} \tag{S11}$$

The second term on the right side of equation (S11) can be written as:

$$\frac{kTln[X_f]}{g_f} = kTln([X_f]^{\frac{1}{g_f}}) \tag{S12}$$

For g_f>>1, $[X_f]^{\frac{1}{g_f}}$ will approach 1 or alternatively $ln[X_f]^{\frac{1}{g_f}}$ will approach zero. Thus, the second

term on the right side of equation (S11) can be neglected for large g_f and we obtain:

$$\Delta G_1^o = \frac{\Delta G^o}{g_f} = kTln[X_1] \tag{S13}$$

Here ΔG_1^o and ΔG^o represent the standard free energy change per surfactant molecule and per micelle, respectively. We note here that k_1 and $[X_1]$ must be converted to mole fractions (dimensionless quantities) prior to evaluation of the logarithm in equation (S13).

Section 3. Formation of polymer—surfactant complexes.

Similar to the formation of free micelles (equation (S2) and (S3)), the formation of polymer—surfactant complexes can be described as a stepwise process, namely:

$$X_1 + X_b \overset{k_b}{\leftrightarrow} X_{1-b} \tag{S14}$$

$$X_1 + X_{1-b} \overset{k_b}{\leftrightarrow} X_{2-b} \tag{S15}$$

……

or alternatively, the overall process can be written as:

$$g_b X_l + X_b \overset{k_2}{\leftrightarrow} X_{g_b-b} \tag{S16}$$

where X_b denotes empty binding sites on the polymer, X_{g_b-b} denotes binding sites occupied by surfactants (with aggregation number g_b), X_p denotes polymers, p is the number of binding sites per polymer chain, k_b is the equilibrium constant for each step (assumed to be constant), and k_2 is an equilibrium constant for the overall process leading to the formation of polymer—surfactant complexes.

From equation (S16), we can write:

$$k_2 = \frac{[X_{g_b-b}]}{[X_1]^{g_b}[X_b]} \tag{S17}$$

and the concentration of surfactants in polymer—surfactant complexes can be written as:

$$g_b\left[X_{g_b-b}\right] = g_b \frac{[X_{g_b-b}]}{total\ binding\ sites} \times total\ binding\ sites \tag{S18}$$

The concentration of all binding sites (capacity of the polymers for surfactant binding) can be written as:

$$[binding\ sites] = p\left[X_p\right] = \left[X_{g_b-b}\right] + [X_b] \tag{S19}$$

Substitution of (S19) into (S18), and then (S17) into (S18) leads to:

$$g_b[X_{g_b-b}] = g_b \frac{[X_{g_b-b}]}{[X_{g_b-b}]+[X_b]} \times p[X_p]$$

$$= g_b \frac{1}{1+\frac{[X_b]}{[X_{g_b-b}]}} \times p[X_p]$$

$$= g_b \frac{1}{1+\frac{1}{k_2[X_1]^{g_b}}} \times p[X_p]$$

$$= g_b p[X_p] \frac{k_2[X_1]^{g_b}}{k_2[X_1]^{g_b}+1} \quad \text{(S20)}$$

Thus, the total concentration of surfactant (in the presence of polymer) can be evaluated as:

$[X_{total}]$ = [singly dispersed surfactant] + [surfactant in free micelles] + [surfactant in polymer—surfactant complexes]

$$= [X_1] + [X_{micelle}] + [X_{polymer-surfactant}]$$

$$= [X_1] + g_f(k_f[X_1])^{g_f} + g_b p[X_p] \frac{k_2[X_1]^{g_b}}{k_2[X_1]^{g_b}+1} \quad \text{(S21)}$$

Section 4 Derivation of ΔG_1^0 expression for formation of polymer—surfactant complexes.

Here we assume that the CAC of the polymer—surfactant complex is much lower than the CAC of surfactant alone. At a concentration between these two CACs, equation (S21) can be written as:

$[X_{total}]$ = [singly dispersed surfactant] + [surfactant in polymer—surfactant complexes]

$$= [X_1] + [X_{polymer-surfactant}]$$

$$= [X_1] + g_b p[X_p] \frac{k_2[X_1]^{g_b}}{k_2[X_1]^{g_b}+1} \quad \text{(S22)}$$

Similar to equation (S9), we can write

$$\Delta G^o = -kTlnk_2 \quad \text{(S23)}$$

Substitution of equation (S17) into (S23) leads to:

$$\Delta G^o = -kTln\frac{[X_{g_b-b}]}{[X_1]^{g_b}[X_b]}$$

$$= g_b kTln[X_1] - kTln[X_{g_b-b}] + kTln[X_b] \quad \text{(S24)}$$

From equation (S19) and (S20), we can write:

$$[X_{g_b-b}] = p[X_p] \frac{k_2[X_1]^{g_b}}{k_2[X_1]^{g_b}+1} \text{ and } [X_b] = p[X_p] \frac{1}{k_2[X_1]^{g_b}+1} \quad \text{(S25)}$$

Here we define $\Theta = \frac{k_2[X_1]^{g_b}}{k_2[X_1]^{g_b}+1}$, which represents the percentage of binding sites on the polymer

occupied by the surfactant. Thus, equation (S25) becomes:

$$\left[X_{g_b-b}\right] = p\left[X_p\right]\theta \text{ and } [X_b] = p\left[X_p\right](1-\theta) \tag{S26}$$

Substitution of equation (S26) into (S24) leads to:

$$\begin{aligned}\Delta G^o &= -kTln\left\{p\left[X_p\right]\theta\right\} + g_f kTln[X_1] + kTln\left\{p\left[X_p\right](1-\theta)\right\} \\ &= g_f kTln[X_1] + kTln\left(\frac{1-\theta}{\theta}\right)\end{aligned} \tag{S27}$$

By dividing both sides of equation (S27) by g_b, we obtain:

$$\frac{\Delta G^o}{g_b} = kTln[X_1] + \frac{kTln\left(\frac{1-\theta}{\theta}\right)}{g_b} \tag{S28}$$

When g_b>>1, the second term on the right side of equation (S28) is negligible, and (S28) can be simplified to:

$$\Delta G_1^o = \frac{\Delta G^o}{g_b} = kTln[X_1] \tag{S29}$$

which has the same form as equation (S13).

Section 5. Self-assembly of amphiphiles in topological defects in LCs.

In this section, we adapt the above described model for polymer—surfactant complexation to describe the concentration-dependent self-assembly of BODIPY-C5 in LC defects. In this analogy, the core of the defect plays the role of the polymer described above. Similar to equation (S16), we assume that the overall process for self-assembly of amphiphiles with defects can be written as:

$$g_d\, X_1 + X_{empty-d} \overset{k_d}{\leftrightarrow} X_{g_d-d} \tag{S30}$$

in which $X_{empty-d}$ denotes unoccupied "binding sites" for amphiphilic assemblies of aggregation number g_d in LC defects. The total number of binding sites is denoted by X_d ($[X_d]$=$\left[X_{empty-d}\right]$ +$\left[X_{g_d-d}\right]$) and thus the maximum capacity of the defects of host amphiphiles is $g_d[X_d]$. The actual number of amphiphiles in the defects at a given concentration is $g_d\left[X_{g_d-b}\right]$, and k_d is the equilibrium constant describing the distribution of amphiphiles between the singly dispersed state in the LC and the assemblies formed in the LC defects.

From equation (S22) and (S30), we can write:

$[X_{total}]$ = [singly dispersed amphiphile] + [amphiphile in assemblies in LC defects]

$= [X_1] + \left[X_{defect}\right]$

$$= [X_1] + g_d[X_d]\frac{k_d[X_1]^{g_d}}{k_d[X_1]^{g_d}+1} \quad \text{(S31)}$$

We comment here that in equation (S31) we exclude the free micelles term shown in equation (S21) because BODIPY-C5 did not form assemblies in the bulk LC over the concentration range that we investigated (see above).

Next, we sought to determine the parameters in equation (S31). We considered a 1 cm-length of a line defect (with core diameter of ~ 10 nm) in a sample of size 1 cm × 1 cm × 80 μm. The number of mesogens localized within the defect core when divided by the total volume of the system provides the apparent concentration of mesogens within the system that are within defects

$$[X_{5CB\ in\ defect}] = \frac{volume\ of\ defect}{volume\ of\ bulk} \times \frac{mass\ density\ of\ 5CB}{molecular\ weight\ of\ 5CB} =$$

$$\frac{1cm\times\pi\times(5nm)^2}{1cm\times1cm\times80\mu m} \times \frac{1008g/L}{249.35g/mol} \sim 10^{-9}\ \text{M} \quad \text{(S32)}$$

When amphiphiles self-assemble in the defect region, mesogens are displaced to the bulk LC. In our simple model, because the sizes of the amphiphiles and mesogens are similar, we estimate the maximum concentration of amphiphiles in the defects (capacity of defect) as [$X_{5CB\ in\ defect}$] ($g_d[X_d] = [X_{5CB\ in\ defect}]$). Furthermore, we assume g_d is 100 (i.e., $g_d \gg 1$), which allows us to estimate the concentration (based on the system volume) of binding sites in defects ([X_d]) as:

$$[X_d] = \frac{[X_{5CB\ in\ defect}]}{g_d} = \sim 10^{-11}\ \text{M} \quad \text{(S33)}$$

We note that our conclusions below are not dependent on the exact value assumed for g_d. As described in the main text, we propose that self-assembly of amphiphiles within LC defects is dominated by the free energy gain associated with transfer of the amphiphile tails from the bulk LC to the assemblies and the replacement of the mesogens in the cores of LC defects by the assemblies. Past studies of the self-assembly of amphiphiles in aqueous solutions have reported that [X_1] largely ceases to increase with [X_{total}] above the CAC[6-13,15-17]. In contrast to this signature of self-assembly, inspection of the monomer signal in Fig. 2 and 3 of the main text reveals that the concentrations of singly dispersed BODIPY-labeled amphiphiles increase at the same rate above and below the CAC. We hypothesized that the behavior of the BODIPY-labeled amphiphiles seen in Fig. 2 and 3 in the main text reflects the fact that the defect cores contain a gradient in ordering of mesogen and thus offer a range of environments in which surfactants can self-assemble. Specifically, the cores of defects possess a continuous gradient in molecular order

and we hypothesized that this leads to growth of the amphiphilic assembly with increasing concentration (above the CAC of 59 μM for BODIPY-C5). To explore the self-assembly behavior predicted by such a model, we arbitrarily considered the LC defects to define ten discrete environments (*m*=10, indicating 10 CACs were defined between the onset of association of BODIPY-C5 (59 μM) and the concentration at which we measured BODIPY-C5 to saturate LC defects (220 μM); the conclusions are unchanged by assuming a different number of environments). We account for this heterogeneity, by defining a series of equilibrium constants:

$$k_{d,n} = e^{\frac{-\Delta G^o_{1,n}}{kT}} \text{ and } \Delta G^o_{1,n} = kTlnCAC_n \quad \text{(S34)}$$

For simplicity, we assume that each environment defined by the defect possesses the same capacity to host amphiphiles ($g_d[X_d]/10 = 1 \times 10^{-10}$ M) with g_d of 100.

Based on the above assumptions, the model becomes:

$$[X_{total}] = [X_1] + \sum_{n=1}^{m=10} \frac{g_d[X_d]}{10} \frac{k_{d,n}[X_1]^{g_d}}{k_{d,n}[X_1]^{g_d}+1} \quad \text{(S35)}$$

As shown by the red curve in Fig. 3e in the main text, this simple model predicts a linear increase of $[X_1]$ with $[X_{total}]$, consistent with the experimental observations. Furthermore, as shown by the blue curve in Fig. 3e, the model predicts growth of the amphiphilic assemblies within the defects above the CAC, until the defects are saturated. We note here that we also measured the monomer signals of BODIPY-fatty acids in the concentration range 10-950 μM, and found the signal also increased linearly with concentration (similar to the dimer signal shown in Fig. 3a and b).

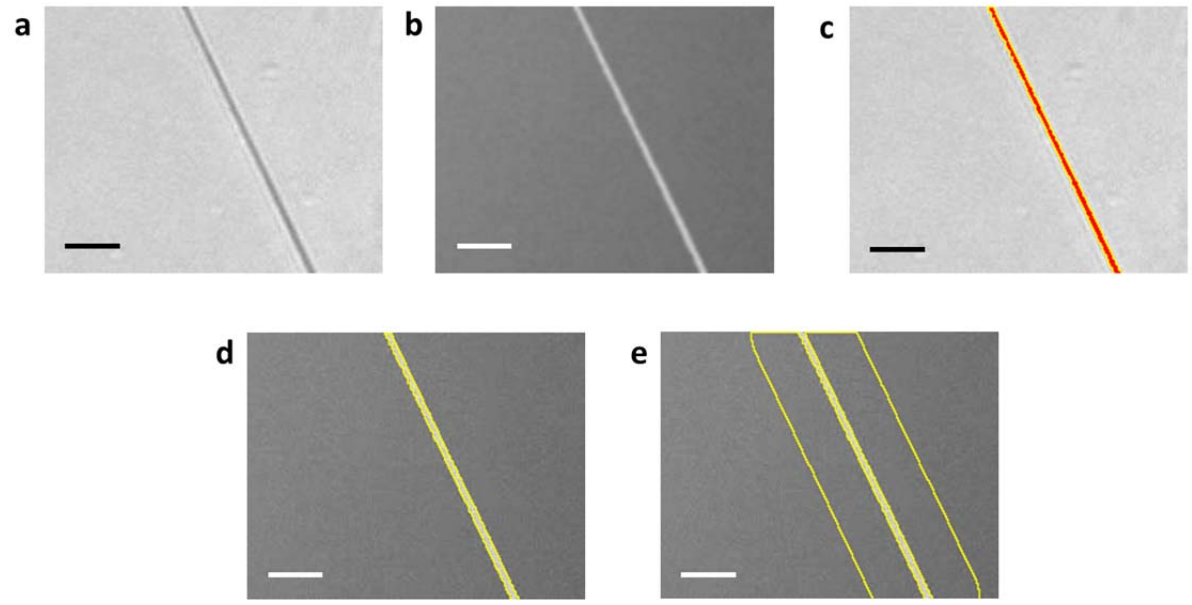

Figure S1 | Quantification of fluorescence intensity. Method to quantify the fluorescence intensity within -1/2 disclination lines and within the bulk of LCs. **a**,**b**, Original bright field (**a**) and fluorescence micrographs (**b**; λ^{em}: 606-684 nm) showing distribution of BODIPY-DHPE (1.9 μM) in nematic 5CB. **c,** Bright field micrograph showing the selection of the defect region. **d,e**, Fluorescence micrographs showing the selection of the LC defects (**d**) and the bulk region around the -1/2 disclination (**e**). Scale bars, 20 μm.

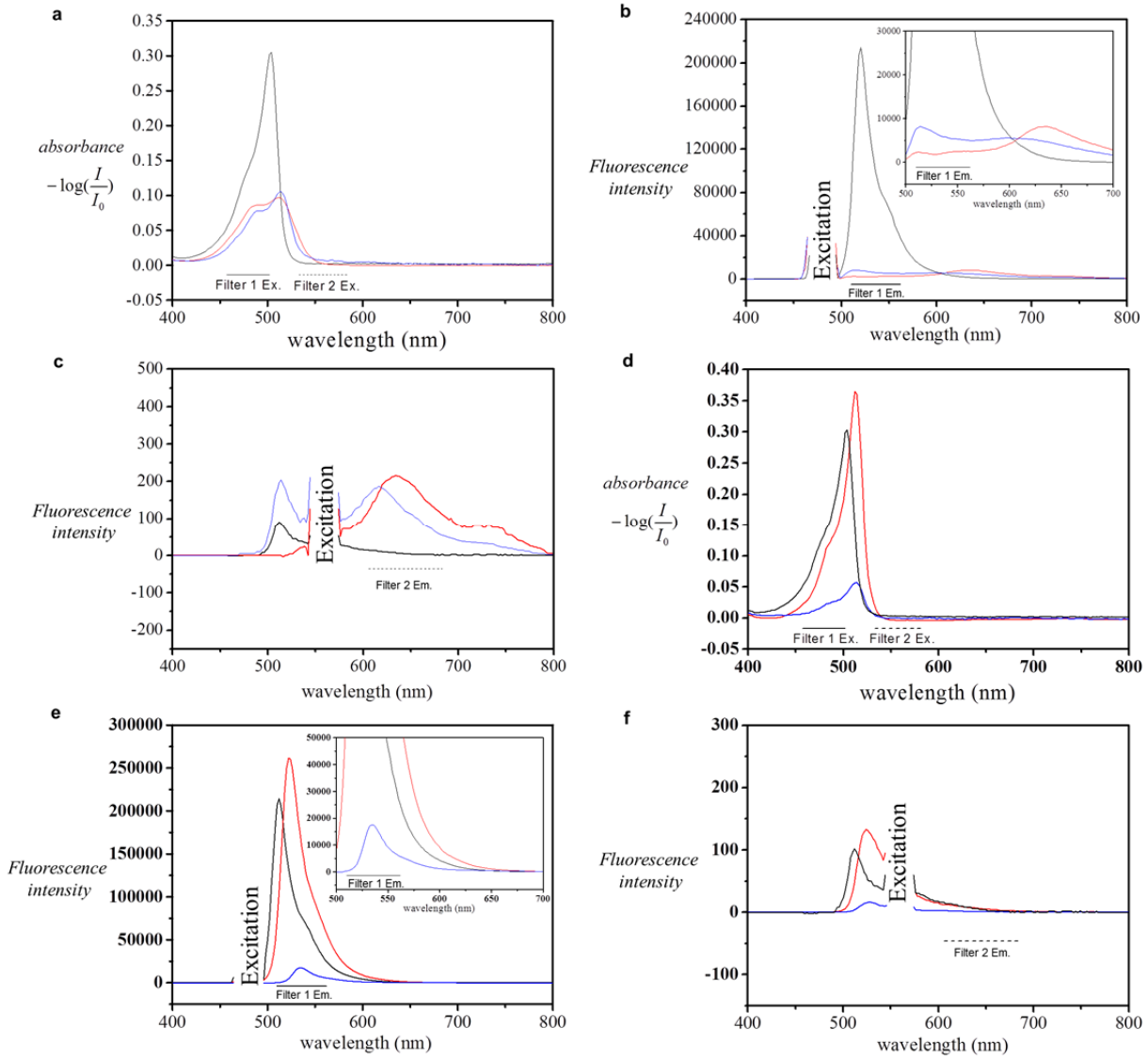

Figure S2 | Absorption and emission spectra of BODIPY amphiphiles. a-c, Absorption (**a**) and emission spectra (**b** and **c**) excited by incident light of 464-494 nm (**b**), and 544-574 nm (**c**) for BODIPY amphiphiles in ethanol or water. The black, red and blue curves represent BODIPY-C5 in ethanol, BODIPY-C12 in water and BODIPY-DHPE in water, respectively. **d-f,** Absorption (**d**) and emission spectra (**e** and **f**) excited by incident light of 464-494 nm (**e**), and 544-574 nm (**f**) of BODIPY amphiphiles in ethanol and isotropic 5CB (39 ^{o}C). The black, red and blue curves represent BODIPY-C5 in ethanol (same curve in **a-c**), BODIPY-C5 in isotropic 5CB and BODIPY-DHPE in isotropic 5CB, respectively. Insets in (**b**) and (**e**) show the curves in the wavelength range of 500-700 nm. The concentration of BODIPY amphiphiles was 3.8 μM. Ex. indicates excitation filter and Em. indicates emission filter.

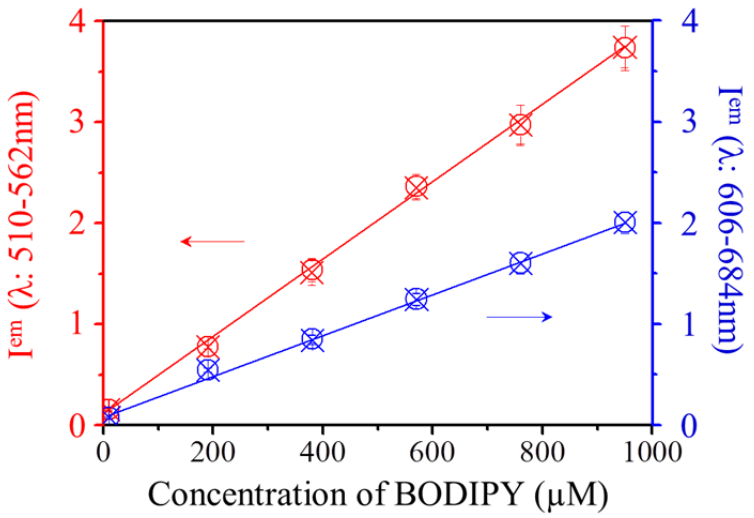

Figure S3 | Rescaled fluorescence intensities of BODIPY in LCs. The solid lines are fits to the fluorescence intensity in the bulk nematic phase. Red: λ^{em} 510-562 nm; Blue: λ^{em} 606-684 nm. ○ in defect, × in bulk. See Method section for actual exposure times. Error bars represent standard deviations and *n*=3 for each data point. One arbitrary unit represents 100,000 (left y-axis) or 2000 (right y-axis) rescaled fluorescence intensity units.

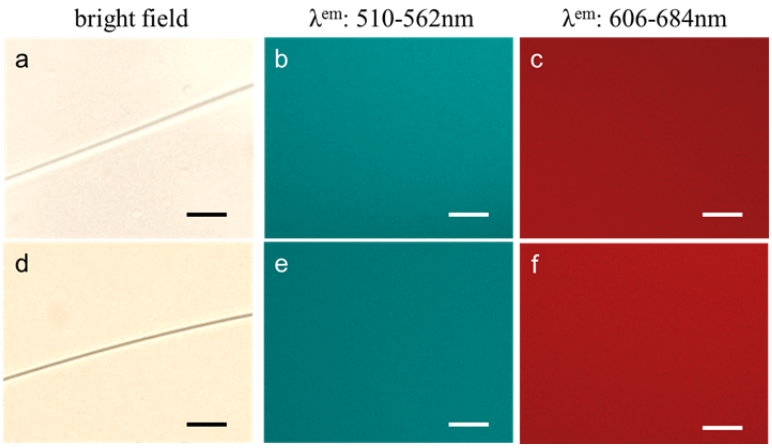

Figure S4 | State of BODIPY-C5 in LCs below CAC. a-f, Bright field (**a,d**) and fluorescence micrographs (**b**,**e**: λ^{em} 510-562 nm; **c**,**f**: λ^{em} 606-684 nm) showing the distribution of BODIPY-C5 (**a-c**: 9.5 µM; **d-f**: 57 µM) in nematic 5CB. Scale bars corresponds to 20 µm.

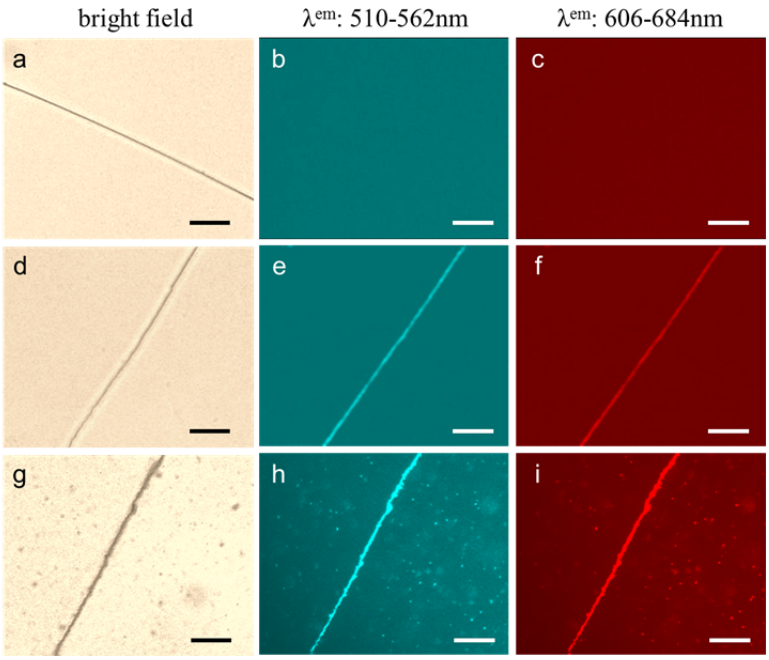

Figure S5 | State of BODIPY-DHPE in LCs. a-i, Bright field (**a,d,g**) and (**b**,**e**,**h**: λ^{em} 510-562 nm; **c**,**f**,**i**: λ^{em} 606-684 nm) fluorescence micrographs showing the distribution of BODIPY-DHPE (**a-c**: 1.3 µM; **d-f**: 1.9 µM; **g-i**: 9.6 µM) in nematic 5CB. Scale bars corresponds to 20 µm.

References

1. Mikhalyov, I., Gretskaya, N., Bergstrom, F. & Johansson, L. B. Electronic ground and excited state properties of dipyrrometheneboron difluoride (BODIPY): dimmers with application to biosciences. *Phys. Chem. Chem. Phys.* **4**, 5663-5670 (2002).
2. Hiemenz, P. S. & Rajagopalan, R. Principles of colloidal and surface chemistry. (CRC, London; 1997).
3. Iliopoulos, I., Wang, T. K. & Audebert, R. Viscometric evidence of interactions between hydrophobically modified poly(sodium acrylate) and sodium dodecyl-sulfate. *Langmuir* **7**, 617-619 (1991).
4. Hansson, P. & Lindman, B. Surfactant-polymer interactions. *Curr. Opin. Colloid Interface Sci.* **1**, 604-613 (1996).
5. Yekta, A., Duhamel, J., Brochard, P., Adiwidjaja, H. & Winnik, M. A. A fluorescent-probe study of micelle-like cluster formation in aqueous-solutions of hydrophobically modified poly(ethylene oxide). *Macromolecules* **26**, 1829-1836 (1993).
6. Biggs, S., Selb, J. & Candau, F. Effect of surfactant on the solution properties of hydrophobically modified polyacrylamide. *Langmuir* **8**, 838-847 (1992).
7. Tanaka, R., Meadows, J., Williams, P. A. & Phillips, G. O. Interaction of hydrophobically modified (hydroxyethyl) cellulose with various added surfactants. *Macromolecules* **25**, 1304-1310 (1992).
8. Guillemet, F. & Piculell, L. Interactions in aqueous mixtures of hydrophobically-modified polyelectrolyte and oppositely charged surfactant- mixed micelle formation and associative phase separation. *J. Phys. Chem.* **99**, 9201-9209 (1995).
9. Piculell, L., Guillemet, F., Thuresson, K., Shubin, V. & Ericsson, O. Binding of surfactants to hydrophobically-modified polymers. *Adv. Colloid Interface Sci.* **63**, 1-21 (1996).
10. Sharma, D. Non-isothermal kinetics of melting and nematic to isotropic phase transitions of 5CB liquid crystal. *J. Therm. Anal. Calorim.* **102**, 627-632 (2010).
11. Nagarajan, R. & Ruckenstein, E. Theory of surfactant self-assembly: a predictive molecular thermodynamic approach. *Langmuir* **7**, 2934-2969 (1991).
12. Rasing, T. & Musevic, I. Surfaces and interfaces of liquid crystals. (Springer, Heidelberg; 2004).

13. Ruckenstein, E., Huber, G. & Hoffmann, H. Surfactant aggregation in the presence of polymers. *Langmuir* **3**, 382-387 (1987).
14. Nagarajan, R. Thermodynamics of nonionic polymer-micelle association. *Colloids Surf.* **13**, 1-17 (1985).